Materials Advances

ROYAL SOCIETY OF CHEMISTRY

PAPER

View Article Online
View Journal | View Issue

Cite this: *Mater. Adv.*, 2023, 4, 3774

Self-textured ZnO *via* AACVD of alkyl alkoxides: a solution-based seed-less route towards optoelectronic-grade coatings†

Clara Sanchez-Perez, *[ab] Sriluxmi Srimuruganathan,[a] Carlos Sotelo-Vazquez, [c] Sanjayan Sathasivam, [ad] Mingyue Wang,[a] Javier Marugán,[c] Ivan P. Parkin [a] and Claire J. Carmalt *[a]

ZnO thin film coatings were synthesised by aerosol-assisted chemical vapour deposition (AACVD) from molecular precursors with different Zn : O ratios, from which synthetic parameters that promote self-texturing were analysed. To that end, the effect of the Zn environment and temperature on the morphology of the resulting ZnO coatings was evaluated for a wide range of synthetic conditions. With the aim to overcome the issues of commercial ZnO precursors, a non-pyrophoric molecular precursor has been investigated to produce 002-oriented, compact, transparent ZnO thin coatings with minimal carbon contamination at 300 °C and fast growth rates (>40 nm min^{-1}). The deposition described herein is a new approach to rapidly achieve coatings at ambient pressure with optimal conditions for optoelectronic applications, and their potential as structural templates to epitaxially grow ZnO in a fast tandem configuration. The results presented in this work provide important insight on the influence of the chemical precursor properties and synthesis conditions to deliver functional ZnO coatings *via* solution-based methods, while obtaining morphologies only achievable by physical vapour deposition techniques.

Received 26th July 2023,
Accepted 30th July 2023

DOI: 10.1039/d3ma00468f

rsc.li/materials-advances

Introduction

Zinc oxide (ZnO) is one of the most studied transition metal oxide materials due to its chemical, physical and electronic properties.[1] The most stable phase of ZnO features a non-centrosymmetrical wurtzite structure, so ZnO crystals can terminate in polar and non-polar surfaces. Interestingly, the surface energy for both surfaces has been claimed to be similar in ZnO, and polar surfaces are anomalously common in comparison to other metal oxides.[2] Due to this, a wide variety of planar and nanostructured ZnO materials are achievable using methodologies that favour growth towards either polar or non-polar directions with variable functionality.[3–5] The directional growth of ZnO nanorods is primarily influenced by the chemical environment surrounding the Zn atoms during the growth process. This is due to the flexible nature of the 3d orbitals of Zn, which allows them to form bonds in either a tetrahedral or planar configuration.[6] The specific arrangement of these bonds determines the directionally of the nanorod growth.[7] Thus, the environment of the Zn first coordination sphere determines the appearance of preferential orientation,[8] leading to non-polar growth in oxygen-deficient conditions while polar growth is favoured in O-rich conditions.[9] Ultimately, the nature of the exposed surfaces plays a key role in the functional behaviour of ZnO,[10] so targeted properties are sought through thorough control of growth conditions.[11] As a result of such functional versatility, its intrinsic n-type doping, its low toxicity and chemical stability, ZnO has been widely used and has elevated prospects in the market of optoelectronic materials,[12] photocatalysis,[13] UV light-emitting-diodes and lasers,[14] solar cell applications,[15] and gas-sensors.[16]

Optoelectronic applications demand coatings with flat surfaces and uniformly distributed and densely packed particles, which requires precise control over film thickness, conformity and morphology.[11,17] Such compact near-to-monocrystalline microstructures are obtained when small crystallites were grown in a single direction,[18] which limits the span of suitable synthetic methodologies. Physical deposition methods can produce said coatings[19,20] as they have negligible carbon intake

[a] *University College London, Department of Chemistry, 20 Gordon St, London WC1H 0AJ, UK. E-mail: c.j.carmalt@ucl.ac.uk*
[b] *Instituto de Energía Solar, Universidad Politécnica de Madrid, 28040 Madrid, Spain. E-mail: c.sanchez.perez@upm.es*
[c] *Department of Chemical and Environmental Technology (ESCET), Universidad Rey Juan Carlos, C/Tulipán s/n, Móstoles, 28933 Madrid, Spain*
[d] *School of Engineering, London South Bank University, London, SE1 0AA, UK*

† Electronic supplementary information (ESI) available. See DOI: https://doi.org/10.1039/d3ma00468f

and the Zn : O ratio can be precisely controlled,[17,21] but they require vacuum conditions, are energy intensive and hard to scale up. In contrast, chemical deposition methodologies are generally faster and can be carried out at atmospheric pressure. Of these, solution-based methods such as sol–gel can use carbon-free reagents, but require stabilising ligands and annealing processes to form crystalline films.[15,22] Therefore, high temperatures are needed to remove the stabilising ligands, which can alter their surface polarity and optoelectronic properties.[6,23] Vapour-phase methods, such as metalorganic chemical vapour deposition (MOCVD), are potentially more advantageous because highly pure and crystalline ZnO coatings are attainable at reasonable reactor temperature ranges during a single step process[24,25] without the need of annealing steps that may trigger surface reconstruction.[6] Still, it should be noted that the choice of precursor and solvent can greatly affect the crystal quality and purity of the resulting film.[26,27] Good-performing precursors for MOCVD of ZnO are currently restricted to volatile but highly corrosive dialkiyl zinc species such as diethyl zinc (DEZ),[28] which require adapted instrumentation and are a fire risk.[29] Thus, the development of non-hazardous and environmentally friendly precursors is therefore of great importance from a manufacturing perspective.

The aerosol-assisted chemical vapour deposition (AACVD) route, in which a mist is created from a precursor solution using a piezoelectric device, widens the range of potential precursors as they need to be soluble rather than volatile.[30] When designing larger precursors for use in processes like AACVD, it is important to consider their decomposition profile to minimise carbon contamination.[31] Additionally, the supersaturation of solvent droplets can lead to multiple nucleation and growth regimes, which further complicates the control of self-texturing and the achievement of uniformly thin coatings.[32] However, by carefully tailoring the design of precursors, it should be possible to overcome these challenges and obtain homogeneously thin coatings through AACVD. Several non-volatile precursors with saturated Zn centres have been investigated due to their high stability and their ability to undergo non-violent thermal decomposition, the most relevant being [Zn(acac)$_2$].[33–36] However, optoelectronic properties of undoped ZnO coatings are still far from those of PVD-grown coatings,[37] and the effect of dopants is insufficient to compete with other transparent conducting oxides (TCOs).[35] This can be explained due to the large amount of carbon content in [Zn(acac)$_2$] that is not easily volatilised upon polymerisation,[38] and the fact that they are partially self-textured with a high amount of grain boundaries. To overcome this issue, directional ZnO coatings can be deposited epitaxially over a seed-layer and/or a template such as c-silicon or c-Al_2O_3,[39–42] however these templates are opaque and/or expensive, and therefore unsuitable for certain applications and large-scale production. It is then of great technological interest to find alternative precursors suitable for AACVD of fully self-textured high purity ZnO thin film coatings without crystallographic templates. To achieve our objective, we investigated the synthetic process and microstructure of ZnO thin films. These films were prepared using solutions containing a pre-organised precursor of zinc alkoxide, which undergoes thermal decomposition to form stable and volatile by-products. Previous reports have suggested that this method is capable of producing thick ZnO coatings that are both crystalline and pure, with a self-textured structure, using AACVD.[30]

Alkyl zinc alkoxides are highly soluble and stable in most aprotic dry organic solvents and, although less reactive than alkyl zinc reagents, they can produce ZnO through a similar path from thermal activation or reaction with water.[43] Their "Zn_4O_4" cubane core is considered as "preorganised" ZnO[16,39] and decompose *via* a polymerisation route that promotes polar growth,[44,45] which determines the shape, size and preferred orientation of the ZnO particles. The ZnO formation rate is correlated to the nature of the alkoxide group, the reaction temperature and the concentration of the solution containing the chemical precursor.[46] However, there is limited insight regarding the nature of the early stages of ZnO nucleation from precursors with pre-organised Zn_4O_4 moieties[47] an how it differs from other common ZnO precursors. Henceforth, understanding nucleation and growth limitations in films deposited from solutions of molecular precursors with different nature is therefore key to design thin film coatings with an intended morphology. In the present work, AACVD was used to study the processes involved in the nucleation and growth of ZnO thin film coatings from Zn(acac)$_2$, DEZ and alkyl zinc alkoxide precursor solutions. Furthermore, the relationship between parameters that enable O-rich or O-poor conditions and precursor is established. It is shown how the use of ethylzinc isopropoxide (EZI) provide great advantages to deliver ZnO coatings with a high degree of grain coalescence, avoiding hazardous alkyl zinc precursors and/or Zn-based precursors with high hydrocarbon content. Through AACVD of EZI, a very thin flat and homogeneous 002-oriented ZnO coating can be deposited even in non-epitaxial substrates, with features comparable to those obtained by PVD techniques.

Experimental

Zinc acetylacetonate (Sigma), diethyl zinc (DEZ) in Hexane (1.0 M anhydrous, Acros Organics) or toluene (1.1 M anhydrous, Sigma) were used as Zn precursors. Methanol (MeOH anhydrous, Sigma) and isopropanol (IPA anhydrous, Acros Organics) were employed as solvents for the synthesis of the ZnO precursors and thin films.

Precursor solutions

Solutions were prepared dissolving 5 mmol of precursor in anhydrous solvent (Table 1). Zn(acac)$_2$ solutions were prepared in 100 mL of MeOH using an ultrasonic bath for 20 min. The DEZ-based precursor solutions were prepared diluting DEZ or DEZ in hexane or toluene, which were mixed with the respective alcohol in the reaction chamber. Ethyl zinc methoxide (EZM) and ethyl zinc isopropoxide (EZI) precursors were prepared following the synthesis method previously published for some of the authors of this work.[45] Briefly, the synthesis consisted of

Table 1 Experimental details for the synthesis of ZnO film coatings from different Zn-based precursors. The temperature of the reaction chamber varied from 300 °C to 500 °C in intervals of 50°. The volume given for each Zn-based precursor is the amount required for complete dissolution and avoidance of pipe blocking during deposition

			Hydrocarbon		Alcohol		Flow	Time	Average growth rate
Precursor	Zn : O ratio	AACVD configuration	Solvent	(mL)	Solvent	(mL)	(L min^{-1})	(min)	(nm min^{-1})
$Zn(acac)_2$	1 : 4	Single-inlet	–		MeOH	*100*	1.2	100	6
DEZ	1 : 0	Dual-inlet	Hexane	*30*	MeOH	*35*	2 × 0.8	20	30
			Toluene	*20*	MeOH	*35*	2 × 0.8	30	20
			Hexane	*30*	IPA	*15*	2 × 0.8	10	60
			Toluene	*20*	IPA	*15*	2 × 0.8	20	30
EZM	1 : 1	Single-inlet	Toluene	*10*	MeOH	*15*	1.8	—	—
EZI	1 : 1	Single-inlet	Hexane	*15*	IPA	*15*	1.8	15	40
			Toluene	*10*	IPA	*15*	1.8	15	40

mixing equimolar amounts of DEZ with anhydrous IPA or MeOH in hydrocarbon solution (hexane or toluene) at −78 °CN. Upon mixing of reagents, the cloudy solution was left stirring under argon for 5 min and then allowed to warm up to room temperature, after which it became transparent.

Thin film growth

Aerosol-assisted chemical vapour deposition (AACVD) was used to synthesise the ZnO thin film coatings. Depositions were carried out in a horizontal cold-walled 17 × 6 cm tubular reactor, either in a single-source or a double-source configuration (Fig. S1, ESI†). After placing the precursor solution mixture in a glass bubbler, an aerosol mist was created using an ultrasonic liquid atomiser (LIQUIFOG, Johnson Matthey) and then transferred to the reaction chamber by flowing nitrogen gas (99.9%, BOC). Silica coated barrier glass was used as substrate to prevent unwanted leaching of ions from the glass, which was cleaned using acetone (99%), isopropanol (99%), and distilled water and dried at 120 °C for 1 h prior to use. ZnO thin film coatings were deposited in the temperature range 300–500 °C, with steps of 50°, and the deposition time varied from 10 to 100 min.

Characterisation

Reactions were carried out in inert conditions using standard Schlenk techniques.[45] Thermogravimetric analyses (TGA/DSC) were carried out in a Netzsch STA 449C instrument using aluminium crucibles in a 20–500 °C range, with the precursor packed under an argon atmosphere or in an oxygen flow. Grazing incidence X-ray diffraction (GIXRD) measurements were performed using a Bruker-Axs D8 (Lynxeye XE) diffractometer with monochromated Cu $K_{\alpha 1}$ radiation (1.54184 Å; 20 kV, 5 mA) at a grazing incident angle of 1°. Diffraction patterns were collected over 20–66° with a step size of 0.05° and a step time of 3 s per point. The surface morphology and film thickness were obtained from top-view and cross-sectional images collected using a JEOL JSM 7600F Field Emission SEM at an accelerating voltage of 5 keV. UV/vis/near-IR transmission spectra were recorded in the 300–2500 nm range using a PerkinElmer Fourier Transform Lambda 950 UV-vis-NIR spectrometer. X-ray photoelectron spectroscopy (XPS) was performed using a Thermo Scientific K-alpha spectrometer with monochromated Al Ka radiation (8.3418 Å) and a dual beam charge compensation system. Survey scans were collected in the range of 0–1200 eV at a pass energy of 50 eV. High resolution peaks were used for the principal peaks of Zn (2p), O (1s), and C (1s), which were modelled using sensitivity factors to calculate relative element concentration within the region of analysis (spot size 400 mm). Peak positions were calibrated to adventitious carbon (284.8 eV) and plotted using the CasaXPS Software.

Results and discussion

Molecular precursors

Pyrophoric DEZ reacts violently with O-containing sources, whereas precursors with pre-formed Zn–O bonds and O : Zn ratios above one – like $Zn(acac)_2$ – undergo a non-violent thermal decomposition. Although thermogravimetric analysis (TGA) of DEZ is not viable, the intermediates of its reaction with alcohols are not pyrophoric, and they can be isolated in an inert atmosphere. In our study, the reaction intermediates of DEZ with methanol and isopropanol are evaluated, namely ethyl zinc methoxide (EZM) and ethyl zinc isopropoxide (EZI), which were synthesised and characterised as recently published by some of the authors.[45] Fig. 1 gathers the TGA of all three precursors in oxidising and inert conditions, alongside the differential scanning calorimetry (DSC) for each thermal process. Fig. 1a shows that $Zn(acac)_2$ decomposes in a narrow temperature range with removal of a large amount of organic non-volatile by-products (over 70% of molecular mass). The observed slight mass uptake until 100 °C could be attributed to a buoyancy effect, common for low-density samples and TGA instruments with a vertical setup.[48] The decomposition pathway of $Zn(acac)_2$ in air exhibits water loss before melting (endothermic steps A and B, respectively), after which full decomposition of the precursor takes place (step C). Although this decomposition profile matches literature data in inert conditions,[49] in strongly oxidizing conditions (such as those met during AACVD) precursor decomposition occurs just below 300 °C.[38] Interestingly, while most DSC analysis reported in the literature fail to show data over 400 °C,[49,50] we observed an exothermic step without significant mass loss at ∼430 °C that can only be attributed to a structural reconfiguration, which

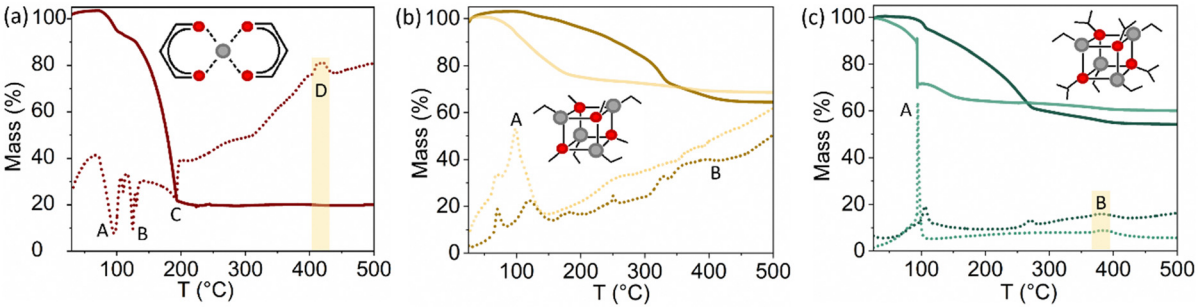

Fig. 1 Thermogravimetric (TGA, full lines) and differential scanning calorimetry (DSC, dotted lines) analyses over the temperature range 25–500 °C of (a) $Zn(acac)_2$ in helium or air, (b) EZM in helium (dark) and air (light) and (c) EZI in helium (dark) and air (light). Atoms of Zn are represented with grey spheres and oxygen with red spheres.

matches with the temperature range of decarbonisation.[51] This is likely the reason to commonly attribute 450 °C as the optimal deposition temperature for ZnO-based coatings formed from $Zn(acac)_2$.[52] Cubane-type precursors EZM and EZI have a far lower organic content (~35% and ~45%, respectively) and different pre-formed bonds so, although the thermal decomposition is driven by a polymerisation process too, different intermediate species are involved.[45] The TGA of EZM (Fig. 1b) shows that the loss of an ethyl group is favoured in contact with an oxygen source (step A, air), but its further decomposition is hindered due to the lack of hydrogen atoms in a β position, preventing by-product release to form crystalline material below 400 °C (step B).

On the contrary, the isopropyl group in EZM (Fig. 1c) enables a β-H elimination process that favours cluster aggregation (step A) and formation of volatile organic by-products that can be carried out through the exhaust.[45] Notably, ZnO formation in helium entails a two-step process triggered by thermal decomposition with complete ZnO crystalline formation below 400 °C (step B), whilst in air EZI suffers additional reaction with O-containing species (moisture). Regardless of pathway, for both EZM and EZI the structural reconfiguration occurs below 400 °C, which suggests that it could be related to diffusion-controlled oxidation of graphitic carbon adsorbed in the thin film[53] rather than the carbonate formation linked to $Zn(acac)_2$ decomposition.

In AACVD the precursor is carried by a solvent to the reactor chamber, typically a mixture of alcohol and hydrocarbon for DEZ and alkoxide solutions.[30] It is noteworthy that the EZM precursor was only stable in toluene/MeOH mixtures at low temperature (−78 °C) and partially decomposed in the bubbler, producing thin films with very low crystallinity (Fig. S2, ESI†). The Zn centres in EZI are more sterically protected than in EZM, so the precursor was stable at RT and could be isolated and stored in an inert atmosphere. Partial decomposition was observed in EZI solutions in anhydrous methanol (MeOH) but was stable in anhydrous isopropanol (IPA). With this palette of precursors and solvent combinations, we have analysed their effect on the Zn : O ratios for Zn coordination sphere during growth and nucleation in ZnO coatings grown in O-poor (Zn : O > 1) and O-rich (Zn : O < 1) conditions.

ZnO thin film coatings

All AACVD-grown ZnO thin film coatings exhibited good substrate coverage with exception of those from $Zn(acac)_2$ solutions at 300 °C and all EZM solutions. Due to the low solubility of $Zn(acac)_2$ in MeOH, diluted solutions and low flow rates were necessary to avoid pipe blocking. Diluted solutions of DEZ were also employed due to its high reactivity with the alcohol in the baffle manifold, which required an additional baffle cooling system. EZI and EZM exhibited good solubility and stability in a wide range of hydrocarbon/alcohol mixtures, making them suitable for use in a single-inlet configuration. This configuration enabled the controlled formation of ZnO thin film coatings, as the precursors reacted and were transformed into ZnO only upon reaching the reaction chamber. This enabled the use of higher precursor concentrations so high flow rates could be used without pipe blockages. As it can be seen in Table 1, the volume of the solvents was optimised to achieve high solubility of the precursors to be fully transferred to the reaction chamber. All reaction parameters are given in Table 1. As-synthesised thin film samples were analysed in sections of 500–600 nm thickness.

Crystallographic analysis of the as-synthesised samples shows that all planes in the range 20–66° belong to the 0001 and $2\bar{1}\bar{1}0$ families of planes in the hexagonal crystal system of Wurtzite ($P6_3mc$). The only visible growth direction from the first family appears due to polar growth along the (002) polar plane along the *c*-axis (002) of the cubic system, whilst the second family appears due to growth in the respectively non-polar [110] and [10*n*] of the cubic system (Fig. 2a). GIXRD results showed that molecular precursors with pre-formed polar Zn–O bonds led to *c*-axis preferential growth (Fig. 2), which was consistent with the existence of O-rich growth conditions.[21] The use of DEZ/hydrocarbon and alcohol solutions in a dual-inlet system led to ZnO thin films with mainly non-polar plane growth when MeOH was employed, which is reported for O-poor synthetic conditions.[21] Interestingly, coatings with mainly polar growth were obtained in similar conditions when IPA was used, suggesting that O-rich conditions are met during the synthesis of the thin film coatings. This effect can be explained by the stabilisation of the EZI intermediate (Scheme 1) that enables ZnO growth *via* small cluster aggregation prior to polymerisation.[45]

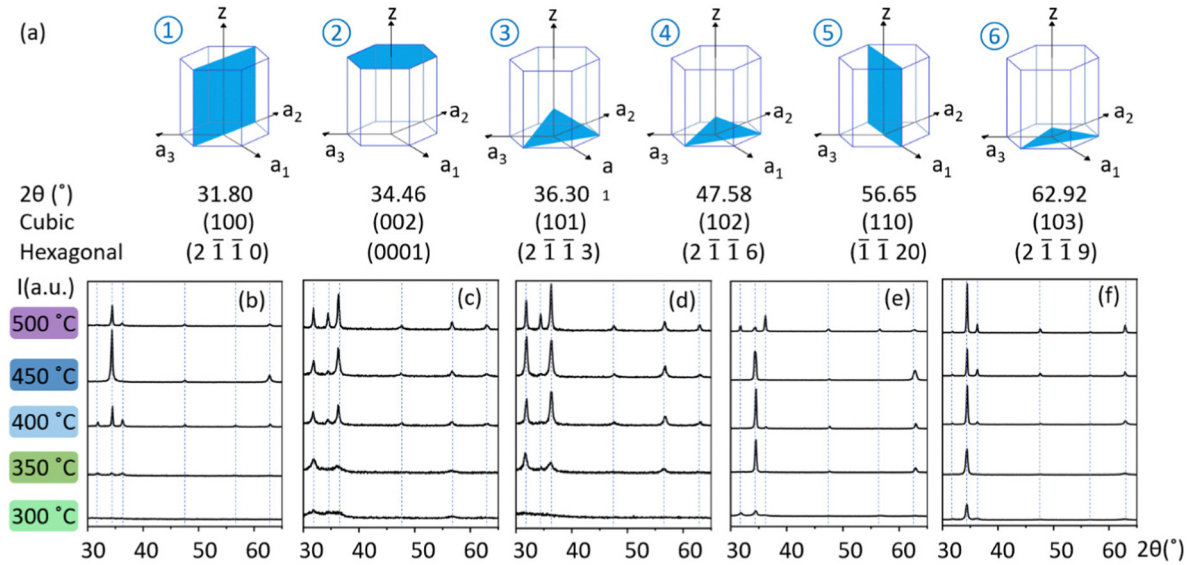

Fig. 2 (a) Schematic representation of the crystallographic planes in the hexagonal unit cell in order of appearance in the diffraction patterns in the 30–66° range and their identity in the cubic and hexagonal system. X-Ray diffraction (XRD) patterns of ZnO thin films grown from (b) $Zn(acac)_2$ in MeOH, (c) DEZ in hexane/MeOH, (d) DEZ in toluene/MeOH, (e) DEZ in hexane/IPA and (f) DEZ in toluene/IPA in the 300–500 °C range at 50° intervals. Blue slashed lines indicate the position of the six diffraction peaks listed in section (a) in order of appearance.

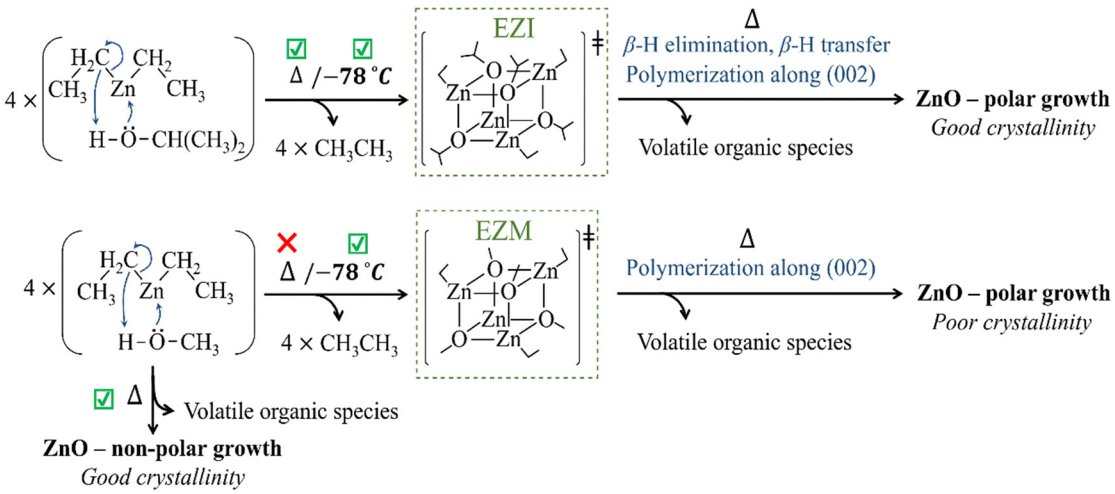

Scheme 1 Reaction pathways for the formation of ZnO thin film coatings from DEZ and MeOH or IPA precursor solutions using the direct mixture of reagents on the hot substrate (dual-source setup, labelled Δ) or a solution of alkoxide stabilised at low temperature (single-source setup, labelled −78 °C).

This statement is supported by the fact that GIXRD patterns of ZnO films grown from isolated EZI solutions were identical to those of films grown from dual-source setups (DEZ in hexane or toluene/IPA) in analogous solvent and temperature conditions (Fig. 2e and f). It is worth noting that for films grown at 500 °C from DEZ in hexane/IPA, the GIXRD pattern indicates polycrystalline nature, which is in good agreement with the μm-sized features observed in Fig. 3. Finally, X-ray diffraction data of coatings deposited from solutions of isolated EZM intermediate also exhibited preferential polar growth (Fig. S2, ESI†), whilst dual-source depositions of DEZ in analogous temperature and solvent conditions exhibited clear non-polar preferred growth (Fig. 2c and d). This implies that the synthetic path for ZnO formation in oxygen-deficient conditions does not involve stabilisation of the tetrameric intermediate at high temperature (Scheme 1), as GIXRD patterns from DEZ/MeOH and EZM solutions with the same co-solvent and deposition temperature were not the same.

Scanning electron microscopy (SEM) was used to study the different morphology shown by the as-deposited ZnO thin film coatings. The different morphology features are due the relative nucleation and growth rates. Micrographs showed a self-texturing effect (Fig. 3), where the surface morphology of the ZnO films can be directly related to their degree of crystallinity and preferential growth. The relative orientation of crystalline planes for the ZnO wurtzite structure is illustrated in Fig. 2a

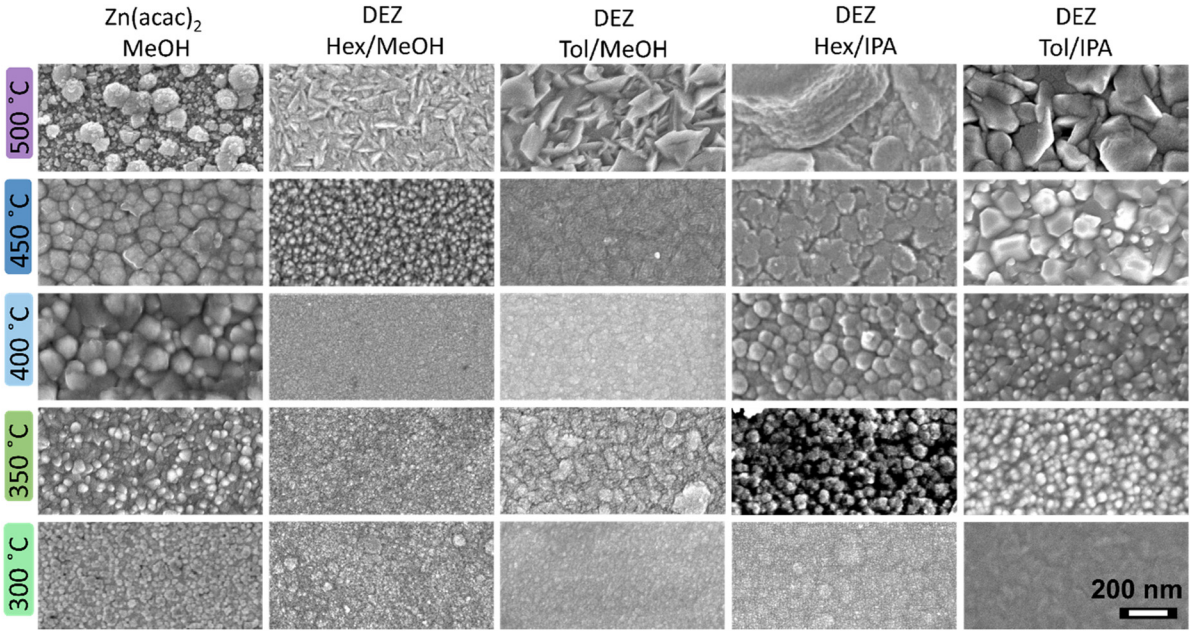

Fig. 3 Scanning electron microscopy (SEM) images of the different ZnO film coatings synthesised from the different Zn-based precursors and solvents at reaction temperatures varying from 300–500 °C. Low reaction temperatures (<400 °C) resulted in ZnO film coatings with grainy or bubble-shape morphology. In contrast, high reaction temperatures (>500 °C) resulted in larger particles. Additionally, the chemical environment of the reaction conditions affected the morphology of the as-synthesised ZnO film coatings, showing wedge-like crystallites under oxygen-deficient conditions, and plate-like crystallites under O-rich conditions.

where the (002) polar plane is parallel to the substrate, whilst planes (100) and (110) are perpendicular to it, and planes in the [10n] direction are oblique to it. Thin film coatings synthesised at low temperature exhibited small and irregular particles with grainy or small bubble-shaped surface features (Fig. 3). Conversely, high reaction temperatures promoted the formation of larger particles with morphologies connected to their respective preferential growth (Fig. 2a). It was observed that thin films synthesised in O-deficient conditions exhibited shallow wedge-like surface crystallites (Fig. 3 (DEZ in Hex/MeOH and DEZ in Tol/MeOH)), a morphology product of the combination of non-polar planes. Instead, thin films gown in O-rich environments promoted the growth of ZnO towards the polar c-axis upon lattice stabilisation due to the filling of oxygen vacancies, forming large blocks and plates parallel to the substrate (Fig. 3 (DEZ in Hex/IPA and DEZ in Tol/IPA)).

SEM micrographs of films grown at 500 °C from DEZ in hexane/IPA exhibited μm-sized features (Fig. 3) which explains the lack of self-texturing (Fig. 2e). Self-texturing above 450 °C was not observed in ZnO coatings prepared from $Zn(acac)_2$ solutions, likely due to adsorption of decomposition by-products causing significant carbon contamination (Fig. S3, ESI†)[38] and resulting in thin films with a bubbly and/or wedgy appearance (Fig. 3). The observed correlation between texturing and thin film morphology in this study provides evidence supporting the idea that the chemical environment at the surface plays a crucial role in stabilising and determining the atomic structure of surface reconstruction.[7] Therefore, it is evident that self-texturing is influenced not only by the deposition temperature of the film,[54] but also by the specific characteristics of the precursor solution used.[55]

It is well-reported that thermal decomposition of precursors with pre-formed Zn–O bonds (O-rich conditions) generate supersaturated proto-nuclei clusters at a large nucleation rate, which are larger than the critical size to evolve as crystallites.[56] This effect is clearly observed in films grown from $Zn(acac)_2$ in which large nucleation sites form and evolve into large and 002-oriented crystallites (Fig. 4). Despite the fast nucleation rate, AACVD of $Zn(acac)_2$ features a slow growth rate, which explains the observed slow film growth. It can be inferred from SEM images that the growth rate is controlled by nucleation at low temperature, and ZnO films are defined by the formation of nano-particular crystallites with no preferred orientation. These synthetic conditions explain the formation of non-equiaxed columnar growth due to the deposition of a partial amorphous phase that led to random nucleation (Fig. 2b). Then, with increasing deposition temperature, crystallite size and crystallinity also increase, and at reaction temperatures slightly above the decarbonisation temperature highly crystalline thin films with equiaxed columnar growth were observed (Fig. 4). Despite this acute self-texturing, organic non-volatile by-products are significantly entrapped in these films, and such contamination hinders their applicability in opto-electronics. Although carbon contamination can be substantially reduced by a short annealing process at 400 °C under O-rich conditions,[53] this has been proved to negatively modify the morphological and optoelectronic features of the as-synthesised ZnO films.[57,58]

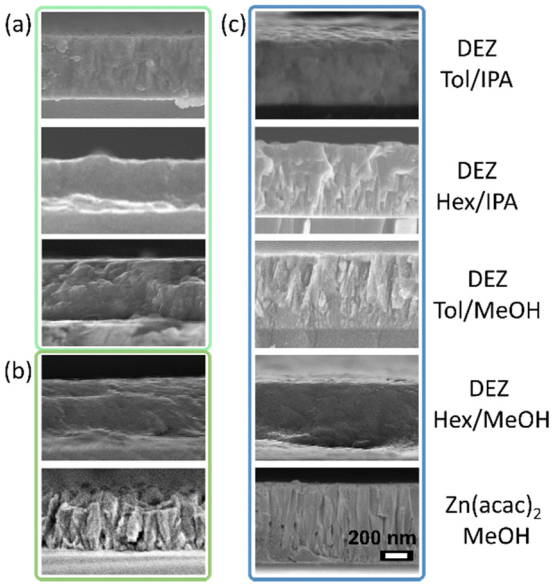

Fig. 4 Cross sectional SEM of ZnO thin films from different precursor solutions at (a) 350 °C, (b) 400 °C and (c) 450 °C, showing that ZnO coatings performed from $Zn(acac)_2$ exhibited columnar growth and low degree of compactness. In contrast, the use of DEZ and EZI resulted in ZnO film coatings with a high degree of grain coalescence, even at low reaction temperatures. Scale bar applies to all micrographs.

In contrast to the previous observation, under O-poor conditions (*e.g.* dual-source CVD of DEZ/MeOH) precursors undergo immediate reaction upon entering the reaction chamber. As a result, the formation of random nucleation sites without significant nuclei proto-clusters is anticipated. Indeed, top-down view and cross-sectional SEM analyses (Fig. 3 and 4) of these thin films show compact coatings without defined crystal boundaries and with high crystallite coalescence, which is consistent with the random formation of small proto-nuclei. The preferred orientation in these films is then expectedly ruled mainly by grain growth towards non-polar directions, and in good accordance with literature.[59] Therefore, in O-poor conditions crystal growth occurs at high supersaturation and not through the formation of a stable intermediate, so it is dominated by slow nucleation rates.

The general morphology of ZnO thin films synthesised from DEZ/IPA is strikingly similar to that of DEZ/MeOH, but their high crystallinity and (002)-preferential growth can only emanate from the formation of small but highly polar proto-nuclei clusters. This effect can be explained by the formation of the stable EZI tetrameric intermediate with Zn–O pre-formed bonds in a cubane-type arrangement. This structure can undergo polymerisation activated through either β-hydrogen elimination or β-hydride transfer, in both cases evolving into *c*-axis oriented proto-nuclei.[45] However, while β-hydrogen elimination produces stoichiometric ZnO, the β-hydride transfer yields oxygen-deficient ZnO_{1-x}, which leads to the formation of smaller nucleation sites. Hence, crystal growth occurs at intermediate supersaturation conditions where crystal nucleation and growth have similar rates, which is consistent with the high degree of crystallite coalescence (Fig. S4, ESI†). Both processes produce highly volatile and stable by-products, which is the driving force for high rate, and the minimal adsorption of these by-products leads to formation of very crystalline nucleation sites.

The optical properties of the as-deposited ZnO thin films were evaluated using UV-Visible spectroscopy. ZnO thin films are optically transparent materials along the solar spectrum with an absorption edge at ~3.3 eV, although their optical properties are affected by the thickness[11] and their crystallinity.[60] The formation of partially amorphous ZnO films can be influenced by the specific conditions employed.[61] This is evident from the observation of an additional blue-shifted optical bandgap in the resulting films.[62,63] Fig. 5 shows how

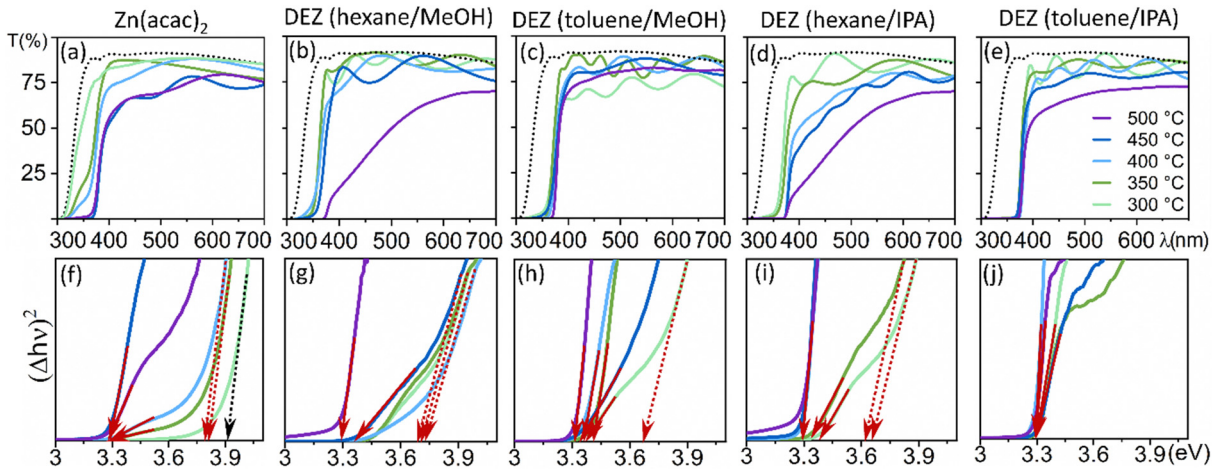

Fig. 5 Transmittance (a)–(e) and band gap calculation using a Tauc[64] plot (f)–(j) of ZnO thin films at reaction temperatures 300 °C (light green), 350 °C (olive), 400 °C (light blue), 450 °C (dark blue) and 500 °C (purple). Dotted black lines represent transmittance of the glass substrate (a)–(e), red arrows represent the bandgap of crystalline ZnO film coatings, red dashed arrows represent the bandgap of amorphous ZnO film coatings and dotted black arrow represents the bandgap of the glass substrate.

the optical properties of ZnO film coatings vary with synthetic conditions, where the bandgap values were calculated using Tauc's formula for direct-bandgap semiconductors.[64]

ZnO coatings grown from $Zn(acac)_2$/MeOH solutions at reaction temperatures below 400 °C exhibit partially amorphous nature, while films deposited above that temperature are crystalline but have low transparency linked to severe carbon contamination (Fig. 5a). Hence, although the use of $Zn(acac)_2$ solutions is convenient, the resulting films have unsuitable optical and electrical properties due to either low crystallinity or low purity. In regard to films grown from DEZ solutions, generally lower transparency was observed in coatings deposited from hexane-containing solutions at high temperature (Fig. 5b and d), making toluene the optimal co-solvent. ZnO coatings obtained from DEZ/MeOH solutions were fully crystalline only above 450 °C, exhibiting high transparency considering they are undoped and their thickness (500–600 nm). Despite the disadvantages associated with the use of DEZ – pyrophoric, low deposition rates –, these synthetic conditions have largely been considered optimal for AACVD of ZnO for optoelectronic applications.[52,59,65] However, the high temperature needed to obtain fully crystalline films hamper their use in numerous advanced functional materials based on heterostructures.[66] Remarkably, coatings deposited from DEZ toluene/IPA solutions were found to be highly transparent and fully crystalline below 350 °C, a substantially lower temperature range than previously reported (Fig. 5e and j). As a result, it has been discovered that fully polar, self-texturing, and crystalline ZnO films can be achieved at temperatures significantly lower (by 100 °C) than those previously reported for AACVD. This finding holds great significance for the advancement of ZnO-based crystallographic templates and heterostructures, opening up new possibilities for their development.[66]

The general conception for ZnO coatings formed *via* AACVD is that dual-source deposition using DEZ/toluene and MeOH produces films with the lowest resistivity,[59] which are grown in O-poor conditions that favour non-polar growth and have high purity.[21] Deposition using $Zn(acac)_2$ or other O-rich single-source precursor produces films with large grains and a mainly polar structure with many facets, which are more resistive and less pure so their functionality is better applied in other fields such as photocatalysis.[13] The cubane-type precursor EZI does fall in between those two conditions, as it is a single-source precursor that provides an O-rich growth environment (β-hydrogen elimination) but can also enable O-poor growth environment (β-hydride transfer). Although it produces polar films that are structurally slightly more resistive than non-polar ones,[21] its decomposition process leads to equally compact films with higher purity than even those from DEZ (Fig. S5, ESI†). Then, the use of ZnO-based materials as TCOs requires adequate microstructure and high purity – both provided in films grown by AACVD of EZI/toluene solutions – as well as doping to boost both optical and electronic materials. In fact, the ability of EZI to produce GZO coatings with enhanced optoelectronic properties was recently reported in the AACVD report published by some of the authors of this work,[45] where films were grown for 15 minutes on glass substrates with prime optoelectronic properties (ρ = 4.7 × 10^{-4} Ω cm; R_{sh} = 9.4 Ω). It this study it was shown that Ga at 3% doping produces self-texturing of ZnO towards the (002) direction, but the formation of exclusively *c*-axis oriented in undoped ZnO coatings is limited to 350 °C (Fig. 2f).

The use of EZI precursor solution offers several advantages, including its non-pyrophoric nature and highly solubility. These properties enable the use of high flow rates, resulting in significantly shorter deposition timeframes. The similar timescale of nucleation and growth allows for the deposition of homogeneous and compact films, which are highly relevant in technological applications such as heterojunctions or as continuous crystallographic template layers. To test the suitability of our synthetic procedure, we conducted a tandem AACVD process using EZI/toluene/IPA as the precursor solution. In this process, a thin fully self-textured layer of crystalline ZnO was first deposited at 350 °C as a ''template'', followed by a deposition at 450 °C. The growth rates were measured at 30–40 nm min^{-1} (Fig. 6a). Initially, we evaluated the feasibility of forming a very thin and uniform layer of ZnO at 350 °C, which is uncommon in solution-processed thin film fabrication.[30] Fig. 6b and c showed the transparent and compact nature of the ZnO template layer, with a homogeneous thickness below 200 nm. When comparing ZnO grown directly on glass at 450 °C to ZnO deposited over the ZnO template layer at the same temperature, it was observed that the latter exhibited full self-texturing towards the *c*-axis (Fig. 6b) without noticeable grain boundaries or interfaces between layers (Fig. 6d). The double-layer ZnO coating also exhibited high transmittance considering it is undoped, although slightly lower due to its increased thickness (Fig. 6e). These results demonstrate the potential of our thin layers as templates for homoepitaxial deposition of ZnO. Moreover, this approach can be extrapolated to enable oriented growth of non-continuous layers as well.

Finally, compositional analysis of selected ZnO coatings was performed using X-ray photoelectron spectroscopy (XPS) after etching (200 s under Ar) to evaluate the bulk film characteristics and obtain a qualitative evaluation of the carbon intake during ZnO formation. For that, the presence and chemical nature of Zn, O and C on ZnO double layers deposited from EZI/IPA/toluene solutions was compared to that of ZnO coatings deposited from precursor solutions of $Zn(acac)_2$ and DEZ in MeOH/toluene at 450 °C. The oxygen 2p environments could be deconvoluted into three separate peaks, O_I and O_{II}, with binding energies of 529.9 eV (±0.2 eV) and 531.6 eV (±0.2 eV), respectively (Fig. 6f). The most intense peak (O_I) can be attributed to O^{2-} ions in ZnO. O_{II} can be attributed to O^{2-} ions located in oxygen deficient regions in ZnO.[67,68] The binding energies of the zinc $2p_{3/2}$ and $2p_{1/2}$ environments were found to be 1021.1 eV (±0.2 eV) and 1044.3 eV (±0.2 eV), respectively, which can be attributed to the Zn^{2+} in ZnO (Fig. 6g).[69,70] Analysis of C1s environment of the ZnO coatings showed that the precursors with unsaturated small ligands with H in β-positions minimised intake of carbon-containing species into the coating (Fig. S5, ESI†). Extremely high levels of carbon

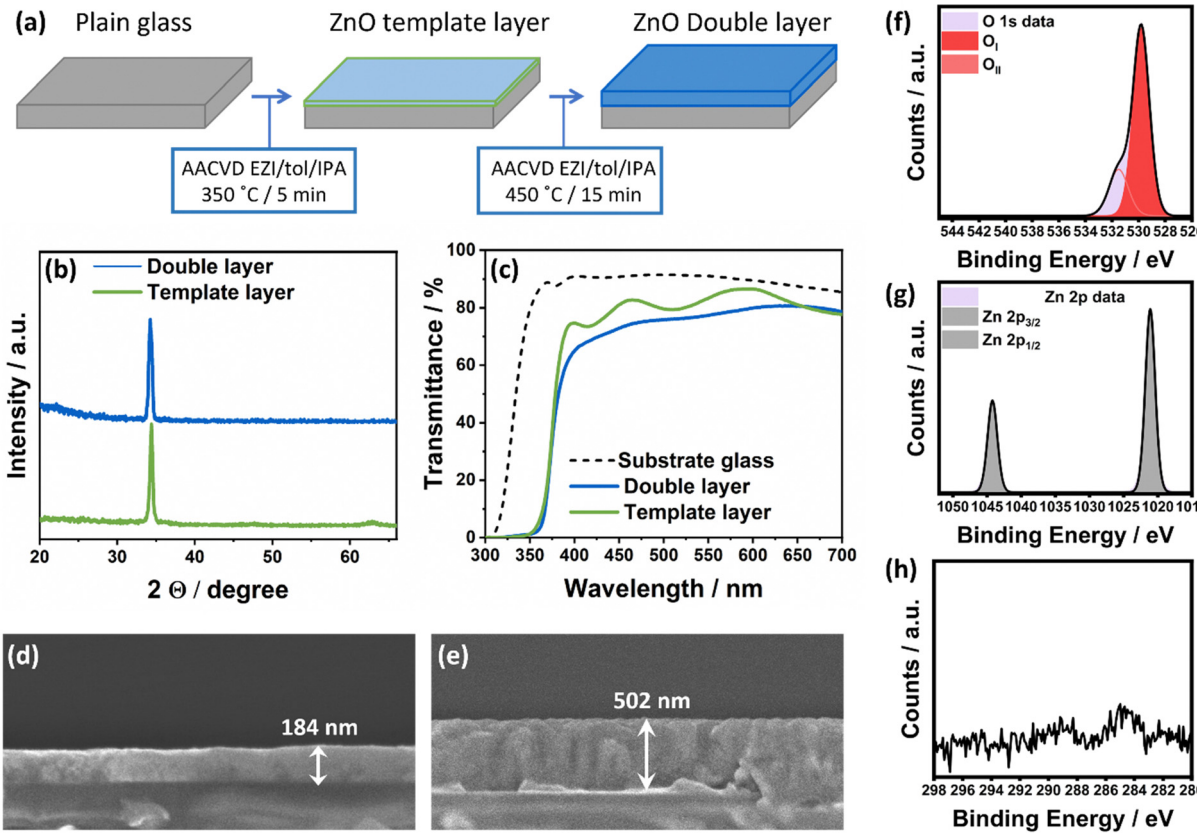

Fig. 6 (a) Schematic representation of the tandem AACVD process proposed for the rapid fabrication of ZnO thin film coatings. (b) GIXRD data of the template layer (bottom) and the ZnO thin film (top) showing uniaxial polar growth and (c) transmittance spectra and band gap calculation using a Tauc[64] plot of the template layer and ZnO thin film made through the tandem deposition process. The transmittance of the substrate glass is included as reference (dotted black line). Cross-sectional SEM images of (d) the template layer grown at 350 °C (184 nm thickness) and (e) the tandem ZnO thin film grown at 450 °C (502 nm thickness). X-ray photoelectron spectroscopy (XPS) spectra of the O 2p environment (f), the Zn 2p environment (g) and the C 1s environment (h) of the ZnO double layer.

contamination (~40%) were found in ZnO coatings from $Zn(acac)_2$ solutions at 450 °C and DEZ solutions, which was not unexpected from mere visual inspection (Fig. S3b, ESI†). Carbon signals amounted to ~4% in films grown from DEZ whilst in the tandem EZI deposition were found within the 1–2% instrumental error of XPS (Fig. 6h). These results confirm that the highly volatile organic by-products produced from decomposition of EZI are better desorbed at lower temperature, favouring minimal contamination during deposition. Thus, we can conclude that our proposed EZI/IPA/toluene precursor solution can successfully generate ZnO coatings with properties suitable for high-end applications[71] through a fast and non-toxic process that requires minimal equipment, showing enormous potential to become the go-to route for fabrication of functional CVD-grown ZnO thin film coatings for TCO applications.

Overall, the novel route to synthesise 002-oriented crystalline template layers with excellent substrate coverage presented herein represents a considerable technological improvement in terms of instrumental resources and time when compared with non-solvent-based methodologies prevalent in industry. Ultimately, the results obtained in this study open an avenue to generate both nanostructure and flat/compact oriented ZnO coatings through an affordable and safely scalable solution-based route.

Conclusions

This paper explores the importance of designing synthesis routes to deliver functional ZnO thin film coatings. The optoelectronic properties of ZnO thin film coatings are greatly affected by purity and morphology, which in turn is determined by synthetic parameters during crystal nucleation and growth. The development of functional ZnO coatings for optoelectronic applications from cost-effective and scalable solution-based methodologies has long been limited by the restricted palette of available molecular precursors. This comprehensive study of the effect of molecular precursors with different Zn : O atomic ratios in different chemical environments aims to shed light into the control of chemical environment of Zn centres during crystal growth. The results of our work show that preferential polar growth is observed in films in which nucleation occurs in O-rich conditions, though the use of a single-source precursor

or from the stabilisation of an intermediate with Zn–O bonds during thin film synthesis. In them, formation of large proto-nuclei creates low supersaturation growth conditions, and nucleation rates are affected by the desorption rate of organic polymerisation by-products. In contrast, preferential growth towards non-polar directions is observed when nucleation occurs in O-poor conditions, where Zn–O bonds are formed during the nucleation process, so no stable intermediate is formed. These specific conditions are met in highly super-saturated solutions, where small nucleation sites are formed leading to densely compact films.

Although ZnO thin films formed in O-poor conditions generally show optimal features for optoelectronic applications, their fabrication through solution-based methods is extremely slow and entails dangers associated to the pyrophoric nature of DEZ. Synthesis of thin film coatings in O-rich conditions is industrially more appealing, however, typical acetylacetonate-based precursors produce ZnO coatings with unsuitable properties for optoelectronic applications, such as low purity and non-compact structures with large crystallites. In this work, the synthesis of ZnO film coatings with similar nucleation and growth rates was achieved from a chemical intermediate of the reaction of DEZ/toluene with IPA. The EZI precursor is not pyrophoric and is stable in inert conditions, and it is highly soluble in hydrocarbon/IPA mixtures, which allows the use of a single-inlet AACVD configuration resulting in a fast and exothermic but non-violent reaction pathway. The synthetic route present in this work therefore avoids blockage issues, resulting in the formation of *c*-axis oriented ZnO thin films with a degree of purity, grain coalescence and transparency comparable to those achieved by PVD methodologies.

This work presents a new synthetic route to produce homogeneous and very thin ZnO film coatings in non-epitaxial substrates through a fast, cost-effective and safely scalable methodology. Importantly, these coatings can further act as structural templates to epitaxially grow ZnO film coatings in a tandem configuration, allowing to rapidly produce prime quality ZnO thin films for optoelectronic applications at ambient pressure.

Conflicts of interest

There are no conflicts to declare.

Acknowledgements

The EPSRC is thanked for funding *via* the Impact Acceleration Account award to UCL 2017–20 (EP/R511638/1) and for grant EP/L017709. The CDT is thanked for funding *via* EP/L015862/1 and NSG is also thanked for providing chemicals and glass substrates. C. S.-V. would like to thank the Regional Government of Madrid for financial support through Programa de Atracción de Talento (2019-T2/AMB-13122) and the Young Researchers R&D Project (Ref. M2727 – Bio-PhLoW) financed by Community of Madrid and Rey Juan Carlos University. M. W. thanks University College London and China Scholarship Council for the joint PhD scholarship.

References

1 D. K. Sharma, S. Shukla, K. K. Sharma and V. Kumar, A Review on ZnO: Fundamental Properties and Applications, *Mater. Today Proc.*, 2022, **49**, 3028–3035, DOI: **10.1016/j.matpr.2020.10.238**.

2 D. Mora-Fonz, T. Lazauskas, M. R. Farrow, C. R. A. Catlow, S. M. Woodley and A. A. Sokol, Why Are Polar Surfaces of ZnO Stable, *Chem. Mater.*, 2017, **29**(12), 5306–5320, DOI: **10.1021/acs.chemmater.7b01487**.

3 A. Mclaren, T. Valdes-Solis, G. Li and S. C. Tsang, Shape and Size Effects of ZnO Nanocrystals on Photocatalytic Activity, *J. Am. Chem. Soc.*, 2009, **131**(35), 12540–12541, DOI: **10.1021/ja9052703**.

4 J. Theerthagiri, S. Salla, R. A. Senthil, P. Nithyadharseni, A. Madankumar, P. Arunachalam, T. Maiyalagan and H.-S. Kim, A Review on ZnO Nanostructured Materials: Energy, Environmental and Biological Applications, *Nanotechnology*, 2019, **30**(39), 392001, DOI: **10.1088/1361-6528/ab268a**.

5 V. Cantelli, S. Guillemin, E. Sarigiannidou, F. Carlá, B. Bérini, J.-M. Chauveau, D. D. Fong, H. Renevier and V. Consonni, In Situ Analysis of the Nucleation of O- and Zn-Polar ZnO Nanowires Using Synchrotron-Based X-Ray Diffraction, *Nanoscale*, 2022, **14**(3), 680–690, DOI: **10.1039/D1NR06099F**.

6 Q. Wang, J. Zhang and C. Song, Stability and Photoelectric Nature of Polar Surfaces of ZnO: Effects of Surface Reconstruction, *Phys. Lett. A*, 2021, **398**, 127274, DOI: **10.1016/j.physleta.2021.127274**.

7 R. Viswanatha, H. Amenitsch and D. D. Sarma, Growth Kinetics of ZnO Nanocrystals: A Few Surprises, *J. Am. Chem. Soc.*, 2007, **129**(14), 4470–4475, DOI: **10.1021/ja068161b**.

8 Y. Kajikawa, Texture Development of Non-Epitaxial Polycrystalline ZnO Films, *J. Cryst. Growth*, 2006, **289**(1), 387–394, DOI: **10.1016/j.jcrysgro.2005.11.089**.

9 R. Salazar, B. Saidi, A. Delamoreanu and V. Ivanova, Electrochemical Growth of Hexagonally Arranged ZnO Nanowall Structures on ZnO Substrates. Influence of Surface Polarity, *J. Electroanal. Chem.*, 2019, **850**, 113397, DOI: **10.1016/j.jelechem.2019.113397**.

10 M. de la Mata, R. R. Zamani, S. Martí-Sánchez, M. Eickhoff, Q. Xiong, A. Fontcuberta i Morral, P. Caroff and J. Arbiol, The Role of Polarity in Nonplanar Semiconductor Nanostructures, *Nano Lett.*, 2019, **19**(6), 3396–3408, DOI: **10.1021/acs.nanolett.9b00459**.

11 T. Singh, T. Lehnen, T. Leuning, D. Sahu and S. Mathur, Thickness Dependence of Optoelectronic Properties in ALD Grown ZnO Thin Films, *Appl. Surf. Sci.*, 2014, **289**, 27–32, DOI: **10.1016/j.apsusc.2013.10.071**.

12 X. Zhao, Q. Li, L. Xu, Z. Zhang, Z. Kang, Q. Liao and Y. Zhang, Interface Engineering in 1D ZnO-Based Heterostructures for Photoelectrical Devices, *Adv. Funct. Mater.*, 2022, **32**(11), 2106887, DOI: **10.1002/adfm.202106887**.

13 P. Dhiman, G. Rana, A. Kumar, G. Sharma, D.-V. N. Vo and M. Naushad, ZnO-Based Heterostructures as Photocatalysts for Hydrogen Generation and Depollution: A Review, *Environ. Chem. Lett.*, 2022, **20**(2), 1047–1081, DOI: **10.1007/s10311-021-01361-1**.

14 B. K. Meyer, H. Alves, D. M. Hofmann, W. Kriegseis, D. Forster, F. Bertram, J. Christen, A. Hoffmann, M. Straßburg, M. Dworzak, U. Haboeck and A. V. Rodina, Bound Exciton and Donor–Acceptor Pair Recombinations in ZnO, *Phys. Status Solidi B*, 2004, **241**(2), 231–260, DOI: **10.1002/pssb.200301962**.

15 H. Liang, Y.-C. Hu, Y. Tao, B. Wu, Y. Wu and J. Cao, Existence of Ligands within Sol–Gel-Derived ZnO Films and Their Effect on Perovskite Solar Cells, *ACS Appl. Mater. Interfaces*, 2019, **11**(46), 43116–43121, DOI: **10.1021/acsami.9b13278**.

16 H. Beitollahi, S. Tajik, F. G. Nejad and M. Safaei, Recent Advances in ZnO Nanostructure-Based Electrochemical Sensors and Biosensors, *J. Mater. Chem. B*, 2020, **8**(27), 5826–5844, DOI: **10.1039/D0TB00569J**.

17 R. R. Kumar, M. Raja Sekhar, K. Raghvendra, R. Laha and S. K. Pandey, Comparative Studies of ZnO Thin Films Grown by Electron Beam Evaporation, Pulsed Laser and RF Sputtering Technique for Optoelectronics Applications, *Appl. Phys. A: Mater. Sci. Process.*, 2020, **126**(11), 859, DOI: **10.1007/s00339-020-04046-8**.

18 T. Minami, H. Sato, K. Ohashi, T. Tomofuji and S. Takata, Conduction Mechanism of Highly Conductive and Transparent Zinc Oxide Thin Films Prepared by Magnetron Sputtering, *J. Cryst. Growth*, 1992, **117**(1), 370–374, DOI: **10.1016/0022-0248(92)90778-H**.

19 B. Szyszka, P. Loebmann, A. Georg, C. May and C. Elsaesser, Development of New Transparent Conductors and Device Applications Utilizing a Multidisciplinary Approach, *Thin Solid Films*, 2010, **518**(11), 3109–3114, DOI: **10.1016/j.tsf.2009.10.125**.

20 P. Płóciennik, A. Zawadzka and A. Korcala, Study of ZnO Thin Film Deposited by PVD, *2015 17th International Conference on Transparent Optical Networks (ICTON)*, 2015, pp. 1–3. , DOI: **10.1109/ICTON.2015.7193661**.

21 N. Fujimura, T. Nishihara, S. Goto, J. Xu and T. Ito, Control of Preferred Orientation for ZnO_x Films: Control of Self-Texture, *J. Cryst. Growth*, 1993, **130**(1–2), 269–279, DOI: **10.1016/0022-0248(93)90861-P**.

22 E. S. Jang, J.-H. Won, S.-J. Hwang and J.-H. Choy, Fine Tuning of the Face Orientation of ZnO Crystals to Optimize Their Photocatalytic Activity, *Adv. Mater.*, 2006, **18**(24), 3309–3312, DOI: **10.1002/adma.200601455**.

23 R. Ghosh, S. Fujihara and D. Basak, Studies of the Optoelectronic Properties of ZnO Thin Films, *J. Electron. Mater.*, 2006, **35**(9), 1728–1733, DOI: **10.1007/s11664-006-0226-6**.

24 S. T. Tan, B. J. Chen, X. W. Sun, M. B. Yu, X. H. Zhang and S. J. Chua, Realization of Intrinsic P-Type ZnO Thin Films by Metal Organic Chemical Vapor Deposition, *J. Electron. Mater.*, 2005, **34**(8), 1172–1176, DOI: **10.1007/s11664-005-0247-6**.

25 A. Nebatti Ech Chergui, C. Pflitsch and B. Atakan, Atmospheric Pressure Metal-Organic Chemical Vapor Deposition (AP-MOCVD) Growth of Undoped and Aluminium-Doped ZnO Thin Film Using Hot Wall Reactor, *Surf. Interfaces*, 2021, **22**, 100883, DOI: **10.1016/j.surfin.2020.100883**.

26 M. Ramya, T. K. Nideep, V. P. N. Nampoori and M. Kailasnath, Understanding the Role of Alcohols in the Growth Behaviour of ZnO Nanostructures Prepared by Solution Based Synthesis and Their Application in Solar Cells, *New J. Chem.*, 2019, **43**(46), 17980–17990, DOI: **10.1039/C9NJ03212F**.

27 *Alcoholic Solvent Influence on ZnO Synthesis: A Joint Experimental and Theoretical Study*, J. Phys. Chem. C. **https://pubs.acs.org/doi/full/10.1021/acs.jpcc.9b07411** (accessed 2023-06-19).

28 S. Nicolay, M. Benkhaira, L. Ding, J. Escarre, G. Bugnon, F. Meillaud and C. Ballif, Control of CVD-Deposited ZnO Films Properties through Water/DEZ Ratio: Decoupling of Electrode Morphology and Electrical Characteristics, *Sol. Energy Mater. Sol. Cells*, 2012, **105**, 46–52, DOI: **10.1016/j.solmat.2012.05.016**.

29 P. Marchand, I. A. Hassan, I. P. Parkin and C. J. Carmalt, Aerosol-Assisted Delivery of Precursors for Chemical Vapour Deposition: Expanding the Scope of CVD for Materials Fabrication, *Dalton Trans.*, 2013, **42**(26), 9406, DOI: **10.1039/c3dt50607j**.

30 C. E. Knapp and C. J. Carmalt, Solution Based CVD of Main Group Materials, *Chem. Soc. Rev.*, 2016, **45**(4), 1036–1064, DOI: **10.1039/C5CS00651A**.

31 P. Marchand and C. J. Carmalt, Molecular Precursor Approach to Metal Oxide and Pnictide Thin Films, *Coord. Chem. Rev.*, 2013, **257**(23), 3202–3221, DOI: **10.1016/j.ccr.2013.01.030**.

32 A. C. Jones and M. L. Hitchman, *Chemical Vapour Deposition: Precursors, Processes and Applications*, Royal Society of Chemistry: Cambridge, UK, 2009.

33 M. R. Waugh, G. Hyett and I. P. Parkin, Zinc Oxide Thin Films Grown by Aerosol Assisted CVD, *Chem. Vap. Depos.*, 2008, **14**(11–12), 366–372, DOI: **10.1002/cvde.200806718**.

34 S. Chen, G. Carraro, D. Barreca, A. Sapelkin, W. Chen, X. Huang, Q. Cheng, F. Zhang and R. Binions, Aerosol Assisted Chemical Vapour Deposition of Ga-Doped ZnO Films for Energy Efficient Glazing: Effects of Doping Concentration on the Film Growth Behaviour and Opto-Electronic Properties, *J. Mater. Chem. A*, 2015, **3**(24), 13039–13049, DOI: **10.1039/C5TA02163D**.

35 S. C. Dixon, S. Sathasivam, B. A. D. Williamson, D. O. Scanlon, C. J. Carmalt and I. P. Parkin, Transparent Conducting N-Type ZnO:Sc – Synthesis, Optoelectronic Properties and Theoretical Insight, *J. Mater. Chem. C*, 2017, **5**(30), 7585–7597, DOI: **10.1039/C7TC02389H**.

36 A. Jiamprasertboon, S. C. Dixon, S. Sathasivam, M. J. Powell, Y. Lu, T. Siritanon and C. J. Carmalt, Low-Cost One-Step Fabrication of Highly Conductive ZnO:Cl Transparent Thin Films with Tunable Photocatalytic Properties via Aerosol-Assisted Chemical Vapor Deposition, *ACS Appl. Electron.*

Mater., 2019, **1**(8), 1408–1417, DOI: 10.1021/acsaelm.9b00190.

37 A. Zaiour, A. Benhaya and T. Bentrcia, Impact of Deposition Methods and Doping on Structural, Optical and Electrical Properties of ZnO-Al Thin Films, *Optik*, 2019, **186**, 293–299, DOI: 10.1016/j.ijleo.2019.04.132.

38 A. V. Ghule, K. Ghule, C.-Y. Chen, W.-Y. Chen, S.-H. Tzing, H. Chang and Y.-C. Ling, In Situ Thermo-TOF-SIMS Study of Thermal Decomposition of Zinc Acetate Dihydrate, *J. Mass Spectrom.*, 2004, **39**(10), 1202–1208, DOI: 10.1002/jms.721.

39 M. Shimizu, T. Shiosaki and A. Kawabata, Growth of C-Axis Oriented ZnO Thin Films with High Deposition Rate on Silicon by CVD Method, *J. Cryst. Growth*, 1982, **57**(1), 94–100, DOI: 10.1016/0022-0248(82)90253-6.

40 Y. R. Ryu, S. Zhu, J. M. Wrobel, H. M. Jeong, P. F. Miceli and H. W. White, Comparative Study of Textured and Epitaxial ZnO Films, *J. Cryst. Growth*, 2000, **216**(1), 326–329, DOI: 10.1016/S0022-0248(00)00434-6.

41 H. Tampo, A. Yamada, P. Fons, H. Shibata, K. Matsubara, K. Iwata, S. Niki, K. Nakahara and H. Takasu, Degenerate Layers in Epitaxial ZnO Films Grown on Sapphire Substrates, *Appl. Phys. Lett.*, 2004, **84**(22), 4412–4414, DOI: 10.1063/1.1758295.

42 V. E. Sandana, D. J. Rogers, F. H. Teherani, P. Bove, M. Molinari, M. Troyon, A. Largeteau, G. Demazeau, C. Scott, G. Orsal, H.-J. Drouhin, A. Ougazzaden and M. Razeghi, Growth of ''Moth-Eye'' ZnO Nanostructures on Si(111), c-Al_2O_3, ZnO and Steel Substrates by Pulsed Laser Deposition, *Phys. Status Solidi C*, 2013, **10**(10), 1317–1321, DOI: 10.1002/pssc.201200975.

43 S. Jana, R. J. F. Berger, R. Fröhlich, T. Pape and N. W. Mitzel, Oxygenation of Simple Zinc Alkyls: Surprising Dependence of Product Distributions on the Alkyl Substituents and the Presence of Water, *Inorg. Chem.*, 2007, **46**(10), 4293–4297, DOI: 10.1021/ic062438r.

44 K. Govender, D. S. Boyle, P. B. Kenway and P. O'Brien, Understanding the Factors That Govern the Deposition and Morphology of Thin Films of ZnO from Aqueous Solution, *J. Mater. Chem.*, 2004, **14**(16), 2575–2591, DOI: 10.1039/B404784B.

45 C. Sanchez-Perez, S. C. Dixon, J. A. Darr, I. P. Parkin and C. J. Carmalt, Aerosol-Assisted Route to Low-E Transparent Conductive Gallium-Doped Zinc Oxide Coatings from Pre-Organized and Halogen-Free Precursor, *Chem. Sci.*, 2020, **11**(19), 4980–4990, DOI: 10.1039/D0SC00502A.

46 C. Lizandara Pueyo, S. Siroky, S. Landsmann, M. W. E. van den Berg, M. R. Wagner, J. S. Reparaz, A. Hoffmann and S. Polarz, Molecular Precursor Route to a Metastable Form of Zinc Oxide, *Chem. Mater.*, 2010, **22**(14), 4263–4270, DOI: 10.1021/cm101240n.

47 K. Sokołowski, I. Justyniak, W. Bury, J. Grzonka, Z. Kaszkur, Ł. Mąkolski, M. Dutkiewicz, A. Lewalska, E. Krajewska, D. Kubicki, K. Wójcik, K. J. Kurzydłowski and J. Lewiński, *Tert*-Butyl(*Tert*-Butoxy)Zinc Hydroxides: Hybrid Models for Single-Source Precursors of ZnO Nanocrystals, *Chem. – Eur. J.*, 2015, **21**(14), 5488–5495, DOI: 10.1002/chem.201406245.

48 E. Hasabeldaim, O. M. Ntwaeaborwa, R. E. Kroon, E. Coetsee and H. C. Swart, Effect of Substrate Temperature and Post Annealing Temperature on ZnO:Zn PLD Thin Film Properties, *Opt. Mater.*, 2017, **74**, 139–149, DOI: 10.1016/j.optmat.2017.03.027.

49 S. Brahma and S. A. Shivashankar, Zinc Acetylacetonate Hydrate Adducted with Nitrogen Donor Ligands: Synthesis, Spectroscopic Characterization, and Thermal Analysis, *J. Mol. Struct.*, 2015, **1101**, 41–49, DOI: 10.1016/j.molstruc.2015.07.075.

50 C. Carra, E. Dell'Orto, V. Morandi and C. Riccardi, ZnO Nanostructured Thin Films via Supersonic Plasma Jet Deposition, *Coatings*, 2020, **10**(8), 788, DOI: 10.3390/coatings10080788.

51 M. Shamsipur, S. M. Pourmortazavi, S. S. Hajimirsadeghi, M. M. Zahedi and M. Rahimi-Nasrabadi, Facile Synthesis of Zinc Carbonate and Zinc Oxide Nanoparticles via Direct Carbonation and Thermal Decomposition, *Ceram. Int.*, 2013, **39**(1), 819–827, DOI: 10.1016/j.ceramint.2012.07.003.

52 D. B. Potter, I. P. Parkin and C. J. Carmalt, The Effect of Solvent on Al-Doped ZnO Thin Films Deposited via Aerosol Assisted CVD, *RSC Adv.*, 2018, **8**(58), 33164–33173, DOI: 10.1039/C8RA06417B.

53 S. S. Nair, T. Saha, P. Dey and S. Bhadra, Thermal Oxidation of Graphite as the First Step for Graphene Preparation: Effect of Heating Temperature and Time, *J. Mater. Sci.*, 2021, **56**(5), 3675–3691, DOI: 10.1007/s10853-020-05481-x.

54 C. Lizandara-Pueyo, M. W. E. van den Berg, A. De Toni, T. Goes and S. Polarz, Nucleation and Growth of ZnO in Organic Solvents - an in Situ Study, *J. Am. Chem. Soc.*, 2008, **130**(49), 16601–16610, DOI: 10.1021/ja804071h.

55 M. H. Koch, A. J. Hartmann, R. N. Lamb, M. Neuber and M. Grunze, Self-Texture in the Initial Stages of ZnO Film Growth, *J. Phys. Chem. B*, 1997, **101**(41), 8231–8236, DOI: 10.1021/jp971088e.

56 J. Zhang, X. Cui, Z. Shi, B. Wu, Y. Zhang and B. Zhang, Nucleation and Growth of ZnO Films on Si Substrates by LP-MOCVD, *Superlattices Microstruct.*, 2014, **71**, 23–29, DOI: 10.1016/j.spmi.2014.03.030.

57 Y. C. Liu, S. K. Tung and J. H. Hsieh, Influence of Annealing on Optical Properties and Surface Structure of ZnO Thin Films, *J. Cryst. Growth*, 2006, **287**(1), 105–111, DOI: 10.1016/j.jcrysgro.2005.10.052.

58 D. Podobinski, S. Zanin, A. Pruna and D. Pullini, Effect of Annealing and Room Temperature Sputtering Power on Optoelectronic Properties of Pure and Al-Doped ZnO Thin Films, *Ceram. Int.*, 2013, **39**(2), 1021–1027, DOI: 10.1016/j.ceramint.2012.07.022.

59 D. S. Bhachu, G. Sankar and I. P. Parkin, Aerosol Assisted Chemical Vapor Deposition of Transparent Conductive Zinc Oxide Films, *Chem. Mater.*, 2012, **24**(24), 4704–4710, DOI: 10.1021/cm302913b.

60 D. Mora-Fonz and A. L. Shluger, Making Amorphous ZnO: Theoretical Predictions of Its Structure and Stability, *Phys. Rev. B*, 2019, **99**(1), 014202, DOI: 10.1103/PhysRevB.99.014202.

61 S. T. Tan, B. J. Chen, X. W. Sun, W. J. Fan, H. S. Kwok, X. H. Zhang and S. J. Chua, Blueshift of Optical Band Gap in ZnO Thin Films Grown by Metal–Organic Chemical-Vapor Deposition, *J. Appl. Phys.*, 2005, **98**(1), 013505, DOI: **10.1063/1.1940137**.

62 H. Maryama and A. Abbassi, Comparative Study of Accurate Experimentally Determined and Calculated Band Gap of Amorphous ZnO Layers, *Mater. Lett.*, 2016, **166**, 206–209, DOI: **10.1016/j.matlet.2015.12.073**.

63 N. Guermat, W. Daranfed and K. Mirouh, Extended Wide Band Gap Amorphous ZnO Thin Films Deposited by Spray Pyrolysis, *Ann. Chim. - Sci. Matér.*, 2020, **44**(5), 347–352, DOI: **10.18280/acsm.440507**.

64 J. Tauc, R. Grigorovici and A. Vancu, Optical Properties and Electronic Structure of Amorphous Germanium, *Phys. Status Solidi B*, 1966, **15**(2), 627–637, DOI: **10.1002/pssb.19660150224**.

65 *Highly conductive and transparent gallium doped zinc oxide thin films via chemical vapor deposition | Scientific Reports*. **https://www.nature.com/articles/s41598-020-57532-7** (accessed 2023-06-21).

66 M. Wang, A. Kafizas, S. Sathasivam, M. O. Blunt, B. Moss, S. Gonzalez-Carrero and C. J. Carmalt, ZnO/BiOI Heterojunction Photoanodes with Enhanced Photoelectrochemical Water Oxidation Activity, *Appl. Catal., B*, 2023, **331**, 122657, DOI: **10.1016/j.apcatb.2023.122657**.

67 C.-F. Yu, S.-H. Chen, S.-J. Sun and H. Chou, Influence of the Grain Boundary Barrier Height on the Electrical Properties of Gallium Doped ZnO Thin Films, *Appl. Surf. Sci.*, 2011, **257**(15), 6498–6502, DOI: **10.1016/j.apsusc.2011.02.051**.

68 S. Chirakkara and S. B. Krupanidhi, Gallium and Indium Co-Doped ZnO Thin Films for White Light Emitting Diodes, *Phys. Status Solidi RRL*, 2012, **6**(1), 34–36, DOI: **10.1002/pssr.201105455**.

69 A. Gulino and I. Fragala, Deposition and Characterization of Transparent Thin Films of Zinc Oxide Doped with Bi and Sb, *Chem. Mater.*, 2002, **14**(1), 116–121, DOI: **10.1021/cm011088y**.

70 S. Karamat, R. S. Rawat, P. Lee, T. L. Tan and R. V. Ramanujan, Structural, Elemental, Optical and Magnetic Study of Fe Doped ZnO and Impurity Phase Formation, *Prog. Nat. Sci.: Mater. Int.*, 2014, **24**(2), 142–149, DOI: **10.1016/j.pnsc.2014.03.009**.

71 J. R. R. Bortoleto, M. Chaves, A. M. Rosa, E. P. da Silva, S. F. Durrant, L. D. Trino and P. N. Lisboa-Filho, Growth Evolution of Self-Textured ZnO Films Deposited by Magnetron Sputtering at Low Temperatures, *Appl. Surf. Sci.*, 2015, **334**, 210–215, DOI: **10.1016/j.apsusc.2014.10.015**.